Self-Aggregation and Supramolecular Structure Investigations of Triton X-100 and SDP2S by NOESY and Diffusion Ordered NMR Spectroscopy

Pavletta S. Denkova,*,†,‡ Luk Van Lokeren,† Ingrid Verbruggen,† and Rudolph Willem†

Vrije Universiteit Brussel, High Resolution NMR Centre (HNMR), Department of Materials and Chemistry (MACH), Pleinlaan 2, B-1050 Brussels, Belgium, and NMR Laboratory, Institute of Organic Chemistry with Centre of Phytochemistry, Bulgarian Academy of Sciences, Acad. G. Bontchev Str., Bl.9, 1113 Sofia, Bulgaria

Received: April 2, 2008; Revised Manuscript Received: June 17, 2008

The self-aggregation and supramolecular micellar structure of two surfactants in aqueous solution, the anionic surfactant SDP2S (sodium dodecyl dioxyethylene-2 sulfate) and the nonionic surfactant Triton X-100 (octylphenol-polyoxyethylene ether with 9.5 ethoxy groups), were investigated by NMR spectroscopy. The critical micellar concentration (CMC), the size, and shape of the aggregates were determined by diffusion ordered NMR spectroscopy (DOSY), while 2D NOESY NMR spectra were used to study the mutual spatial arrangement of surfactant molecules in the aggregated state. A nonlinear increase of the micellar hydrodynamic radius, indicating possible sphere-to-rod shape transition, was found for SDP2S at higher surfactant concentrations. Triton X-100 micelles were found to be almost spherical at low surfactant concentrations, but formation of ellipsoid shaped particles and/or micellar aggregation was observed at higher concentrations. The NOESY data show that at low concentration Triton X-100 forms a two-layer spherical structure in the micelles, with partially overlapping internal and external layers of Triton X-100 molecules and no distinct hydrophilic−hydrophobic boundary.

1. Introduction

The size, shape, and structure of micelles in surfactant solutions are important characteristics in determining their main properties and areas of application. It is known that the size of micelles formed in aqueous surfactant solutions ranges from 10 to 100 Å and that their shape varies upon increasing surfactant concentration. Typically, at the critical micellar concentration (CMC) and at some concentration ranges above, micelles have a spherical, ellipsoid, or cylindrical shape, the corresponding isotropic micellar solutions lacking long-range correlations. At very high concentrations, the micelles grow up to very long chains and can form entangled superstructures (isotropic or nonisotropic) with properties similar to those of polymers in the semidilute regime. In this case, the aggregates extend over microscopic distances and form nondiscrete structures characterized by continuity of the surfactant aggregates in one, two, or three dimensions.[1−3]

Molecular translational mobility, expressed by the translational diffusion coefficient, is very sensitive to aggregation and other inter- or supramolecular interactions, including hydrogen bonding. In micellar solutions, variations in the surfactant diffusion coefficient reflect changes in micellar size and shape, intermicellar interactions, solubilization, and hydration. Investigation of the concentration dependence of a surfactant diffusion coefficient is a widely used approach to obtain quantitative information about micelles.

For many years, NMR spectroscopy has been successfully applied to the investigation of surfactant solutions. Chemical shifts, relaxation times, and scalar coupling constants measured as a function of the surfactant concentration provide information about self-aggregation, CMC, and structure of the micelles, while pulsed field gradient NMR spectroscopy enables one to determine surfactant diffusion coefficients.[3−6] In particular, diffusion ordered NMR spectroscopy (DOSY) grew to a valuable tool for complex mixture analysis.[7,8] The advantage of this approach is that it allows spectroscopic mixture component separation on the basis of their different diffusive behavior.

The present investigation focuses on two individual surfactant systems, the anionic surfactant SDP2S (sodium dodecyl dioxyethylene sulfate) and the nonionic surfactant Triton X-100 (octylphenol-polyoxyethylene ether with averaged 9.5 ethoxy groups, abbreviated TX100). The CMC, size, and shape of the micelles are determined by 2D DOSY, while the mutual spatial arrangement of the surfactant molecules in the aggregates was elucidated by 2D NOESY. No data about CMC and micellar sizes of SDP2S, in the absence of additives, are, to the best of our knowledge, available in the literature. Actually, SDP2S has been studied so far only in the presence of multivalent counterions using light scattering.[9−11]

The choice of TX100 is motivated by the fact that it forms micelles at a relatively low surfactant concentration, offering a wide concentration range in the isotropic liquid region where surfactant molecules form discrete micelles. TX100 solutions have been investigated by various sizing techniques,[12−17] including 1D NMR, making possible comparison of our own DOSY results with the data previously published. The issue about the TX100 micelle shape, however is still open since Robson and Dennis,[12] proposed two possible arrangements, one spherical multilayered and one oblate monolayered, without providing evidence for either possibility. The present paper provides clear-cut data in this respect, based on 2D NOESY spectra.

* To whom correspondence should be addressed. E-mail: psd@orgchm.bas.bg. Phone: +359 (2) 9606 172. Fax: +359 (2) 870 02 25.
† Vrije Universiteit Brussel.
‡ Bulgarian Academy of Sciences.

10.1021/jp802830g CCC: $40.75
Published on Web 08/13/2008

2. Experimental

2.1. Materials. *p-tert*-Octyl-phenyl-polyoxyethylene-(9.5) glycol, with an average of 9.5 oxyethylene units per molecule, $(C_8H_{17}C_6H_4(OCH_2CH_2)_{9.5}OH$ (Triton X-100, Sigma), with MW = 646, was used without further purification. A wide concentration range from 1.5 to 542 mM (0.097 to 35%), within isotropic L1 limits of its phase diagram, was studied. Three samples with concentrations 0.1, 0.05, and 0.01 mM below the CMC (0.24−0.28 mM) were also measured to determine the monomer surfactant diffusion coefficient.

Sodium dodecyl dioxyethylene sulfate (SDP2S), MW = 376, with chemical structure $CH_3(CH_2)_{11}(OCH_2CH_2)_2OSO_3Na$, Empicol ESB70, was used as purchased. The concentrations investigated ranged from 0.05 to 133 mM (0.056 to 5%).

All solutions were prepared with D_2O (99.95%, Aldrich).

2.2. Methods. All diffusion NMR measurements were performed at 300 K on a Bruker Avance DRX 250 NMR spectrometer equipped with a high gradient diffusion probe Diff 30.

2.2.1. DOSY Spectra. The DOSY spectra were acquired with the standard pulse program from Bruker Topspin software, *ledbpgp2s*, using a stimulated echo and the longitudinal eddy current delay, with bipolar sine shaped gradient pulses and two spoiling gradients. All spectra were recorded with 16 K time domain data points in t_2 dimension and 32 t_1 increments, 16 transients for each t_1 increment, and a relaxation delay of 3 s.

Achieving complete sampling of the full signal attenuation range appeared essential for obtaining diffusion coefficients of high accuracy. The issue is acute for systems with an unfavorable combination of fast relaxation and slow diffusion, which is often the case in surfactant solutions, nanoclusters, and other supramolecular aggregates. To determine the optimal combination of experimental parameters for full coverage of the diffusive signal attenuation, we simulated the signal amplitude as a function of the NMR scattering vector q ($q = \gamma\delta G$) using the equation applicable to the pulse program and gradient pulse shape used[18]

$$\frac{I}{I_0} = \exp\left[-D(\gamma\delta G)^2\frac{4}{\pi^2}\left(\Delta - \frac{5\delta}{16} - \frac{\tau}{2}\right) - R\right]$$

where R is the relaxation contribution to signal attenuation, defined as[19]

$$R = 2\frac{\delta + \tau}{T_2} + \frac{(\Delta - \tau - \delta) + T_e}{T_1}$$

τ is the echo time and T_e is the eddy current delay.

For the simulations, a D value of 1×10^{-11} m^2/s and average values of 250 ms for T_1 and 80 ms for T_2 were used on the basis of relaxation data for different molecular fragments of TX100, determined in separate experiments for 9 mM TX100 solution.

Following the simulation results, a compromise diffusion time value Δ of 100 ms was used for all measurements in order to keep the relaxation contribution to the signal attenuation constant for all samples. The gradient pulse length δ was 1 ms except for samples with very low D values, where it was 1.6 ms, in order to ensure full signal attenuation. The gradient pulse strength G was varied in 32 linear steps in the interval from 2 to 45% of the maximum gradient output of the gradient unit (12 *T*/m) and up to 65% for samples with higher concentration. The spectra were first processed in the F2 dimension by standard Fourier transform with 2 K data points and sine squared window function (qsine, ssb = 2). To extract the diffusion dimension, the data set representing the signal attenuation as a function of the NMR scattering vector q^2 ($q = \gamma\delta G$) was subjected to Inverse Laplace Transform using the MaxEnt method implemented in the GIFADOSYm software package integrated in Topspin.[20] The evaluation of the diffusion coefficients was performed by fitting the sum of the columns along the chemical shift of each signal in the DOSY spectrum with the Gaussian distribution curve.

To avoid the dynamic range problems resulting from the strong residual water signal, especially when the surfactant concentration is very low, below or relatively close to the CMC, the standard *ledbpgp2s* DOSY pulse sequence was adapted to include a water presaturation cycle. For a certain range of concentrations, the diffusion coefficients were measured with the two pulse sequences for comparison. The DOSY spectra recorded with water suppression are of better quality, are less noisy, and are more reproducible, even though the values of the diffusion coefficients determined with the two pulse sequences are identical within experimental error.

2.2.2. NOESY Spectra. The 2D NOESY spectra were recorded at three surfactant concentrations, 9, 12, and 77.4 mM, with the standard Bruker program *noesygptp* in the phase-sensitive mode, using States-time-proportional phase incremention (States-TPPI) and sine shaped gradient pulses during the mixing period. The spectra were recorded with a spectral width of 2000 Hz, 1 K data points in the t_2 time domain, and 256 t_1 increments, 32 transients for each t_1 increment, and a relaxation delay of 3 s. The spectra were recorded for each sample with at least 14 different mixing times ranging from 5 to 600 ms to ensure optimal discrimination between direct cross-relaxation and spin-diffusion and to determine the mixing time range where the initial rate approximation holds. A sine window function (ssb = 2) and zero-filling were applied in both dimensions prior to Fourier transformation, to give 2048 × 2048 data matrices in the frequency domain with 0.98 Hz/pt of digital resolution.

3. Results and Discussion

3.1. General Approach for Diffusion Data Analysis.

3.1.1. Determination of CMC. In the low concentration range, the surfactant molecules are in dynamic equilibrium between monomeric and micellar states, which, in most cases, is fast on the chemical shift time scale. The observed chemical shifts are population weighted averages of the chemical shifts in the two states. In this case, the measured diffusion coefficient depends on surfactant molecular dynamics with respect to the diffusion time scale. If the exchange kinetics between the monomeric and micellar states is fast on the diffusion time scale, the measured diffusion coefficient D_{meas} is a population weighted average of the diffusion coefficients of the monomer and the micelle[4]

$$D_{meas} = D^{mic} + \frac{CMC}{C_T}(D^{mon} - D^{mic}) \quad \text{for } C_T > \text{CMC} \tag{1a}$$

$$D_{meas} = D^{mon} \text{ for } \quad C_T \le \text{CMC} \tag{1b}$$

where $D^{mon}$and D^{mic} represent, respectively, the monomer and micellar diffusion coefficients and C_T is the total surfactant concentration.

Equation 1a predicts that at concentrations above the CMC the diffusion coefficient depends linearly on the inverse concentration, $1/C_T$, assuming that the concentration of the monomer is constant and equal to the CMC. At concentrations below the CMC, the measured diffusion coefficient is indepen-

dent of the concentration and equal to the diffusion coefficient of monomers. An overall plot of D_{meas} against $1/C_T$ consists of two straight lines intersecting at $1/C_T = 1/CMC$. The extrapolation of the line above the CMC to $1/C_T \rightarrow 0$ gives the value of D^{mic}. When the values of the CMC and D^{mon} are known, D^{mic} can be directly determined from eq 1a. When the concentration of the monomer is not negligible, the value of D_{meas} should be corrected according to eq 1a to obtain the diffusion coefficient of the micellized surfactant D^{mic}.

3.1.2. Determination of Micellar Size and Shape. The micellar diffusion coefficient D^{mic} can be used to assess the size and shape of the aggregates.

The simplest model uses the Stokes−Einstein equation to derive the hydrodynamic radius, R_h

$$D = \frac{kT}{6\pi\eta R_h} \tag{2}$$

where η is the solvent viscosity, $\eta(D_2O) = 1.0511$ cP at 300 K (NIST, USA), which assumes that the particles are perfectly spherical and noninteracting, hence solely subject to solvent friction.

When particles are much larger than solvent molecules, as is the case in micellar solutions, $R_h = R_{h,app}$ is considered as the apparent hydrodynamic radius of a fictitious spherical particle that would have the same diffusion coefficient. This holds in particular at higher surfactant concentration where ellipsoid aggregates normally form. Various shape functions can then be applied to translate the measured diffusion coefficient into geometrical parameters of the aggregate.

For ellipsoid aggregates, the following general equation applies[21]

$$D = \frac{kT}{6\pi\eta b} f(\rho) \tag{3}$$

where b is the minor semiaxis length of the micelle; $\rho = a/b$ is the axial ratio, with a being the length of the major semiaxis; and $f(\rho)$ is a function representing the shape factor.

For a prolate ellipsoid, eq 4 holds

$$f(\rho) = \frac{\ln(\rho + \sqrt{\rho^2 - 1})}{\sqrt{\rho^2 - 1}} \tag{4}$$

while for an oblate ellipsoid eq 5 is used

$$f(\rho) = \frac{\arctan(\sqrt{\rho^2 - 1})}{\sqrt{\rho^2 - 1}} \tag{5}$$

3.1.3. Obstruction Effects and Intermicellar Interactions. At higher surfactant concentrations, the measured diffusion coefficient is a function of both the micellar size and intermicellar interactions, which can also contribute to decreasing the diffusion coefficient, due to the increased micellar volume fraction. To account for the particle obstruction in a system of interacting monodisperse hard spheres with no hydrodynamic interactions, the concentration dependence of the micellar diffusion coefficient is usually given to a first-order approximation in micelle volume fraction by the following expression[22]

$$D^{mic} = D_0^{mic}(1 - k\Phi) \tag{6}$$

where Φ is the volume fraction of the micelles; D_0^{mic} is the micellar self-diffusion coefficient at infinite dilution in the absence of intermicellar interactions; and k is a dimensionless constant, which depends on the aggregate geometry and interactions. It was theoretically derived[22] and experimentally proven[3,23,24] that for spherical particles k lies in the range 2−2.5. Deviation from this range is a qualitative indication that the micelles are not spherical. Spherical micelle diffusion will be less hindered by the other micelles than oblate or prolate aggregates.

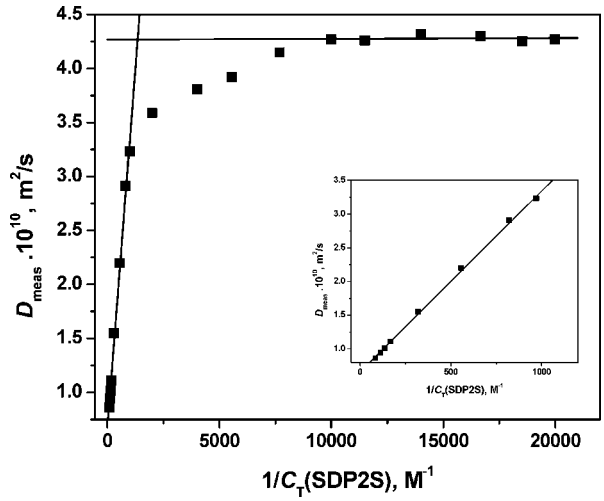

Figure 1. Measured diffusion coefficient, D_{meas}, as a function of the reciprocal of SDP2S concentration ($1/C_T$) (statistics for the inset, $R^2 = 0.9988$, SD $= 3.4568 \times 10^{-12}$, $N = 8$, Int $= 6.6 \pm 0.4 \times 10^{-11}$, slope $= 2.7 \pm 0.08 \times 10^{-13}$).

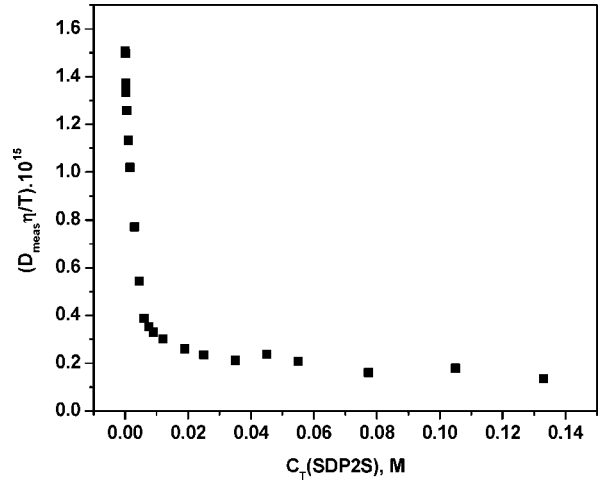

Figure 2. Plot of the normalized diffusion coefficient as a function of the total SDP2S concentration for the concentration range above the CMC.

3.2. Sodium Dodecyl Dioxyethylene Sulfate (SDP2S). Figure 1 represents a plot of the measured diffusion coefficient of SDP2S against the reverse total surfactant concentration, ($1/C_T$), and the respective linear fits of the experimental data according to eq 1. This approach implicitly assumes that the size of the micelle is changing, for a constant given shape. The CMC value of SDP2S determined under these conditions from our data is 0.8 mM.

Figure 2 shows a plot of $D_{meas}\eta/T$ against SDP2S concentration, in the concentration range above CMC from 1.5 to 133 mM. The fast decrease of the diffusion coefficient at concentrations above but still close to CMC implies a significant presence of monomer fraction. A linear fit of the data above 12 mM and extrapolation to $C_T = 0$ gives the diffusion coefficient at infinite dilution, $D_0^{mic} = 7.78 \times 10^{-11}$ m^2/s, which provides a hydrodynamic radius R_h of 2.69 nm. This radius is in excellent agreement with the total length of the surfactant molecule 2.77 nm, calculated as the sum of the lengths of the extended

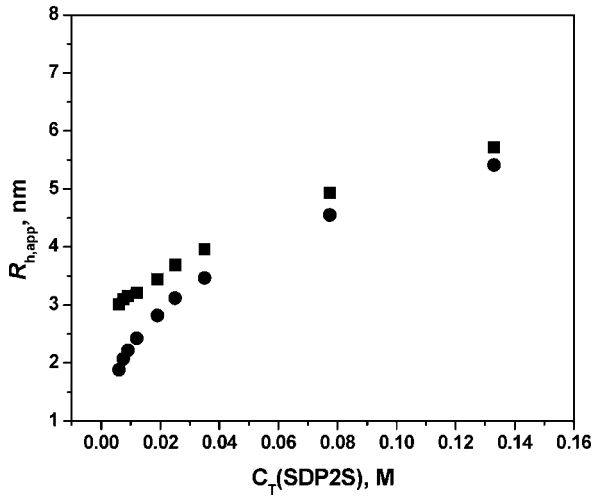

Figure 3. Apparent hydrodynamic radius of SDP2S micelles, $R_{h,app}$, as a function of surfactant concentration, calculated using directly the measured diffusion coefficient, D_{meas} (dots), or the micellar diffusion coefficient, D^{mic} (squares).

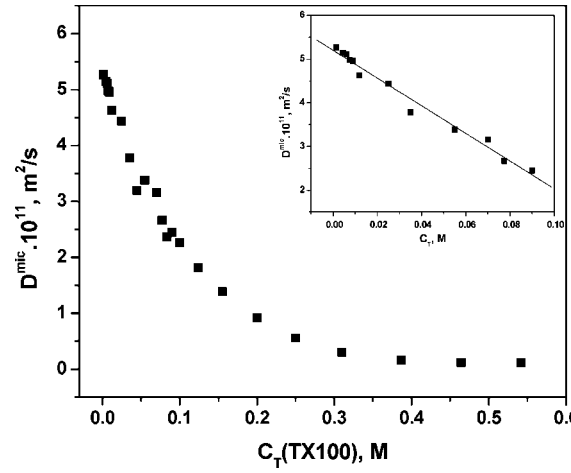

Figure 4. Micellar diffusion coefficients D^{mic} as a function of TX100 concentration. The inset represents the low concentration range up to 75 mM, where a linear dependence of D^{mic} is observed ($R^2 = 0.9810$, Int $= 5.20 \pm 0.06 \times 10^{-11}$; Slope $= -3.2 \pm 0.1 \times 10^{-10}$, $N = 12$, SD $= 1.4859^{-12}$).

conformation of the hydrocarbon chain and of the hydrophilic chain moiety, including the two oxyethylene groups and the $-OSO_3^-$ anion, respectively, 1.65 and 1.12 nm.

The aggregation number was estimated as the ratio of the total volume of the hydrophobic micelle core, V_{core} (16.83 nm^3), and the volume of the hydrophobic tail of a single surfactant molecule, V_{tail} (0.375 nm^3). The volume of the micelle hydrophobic core was calculated from eq 7[11]

$$V_{core} = \frac{4\pi(R_{h,0} - l_{head})^3}{3} \quad (7)$$

where l_{head} is the length of the hydrophilic head (1.12 nm). Using the molecular weight of the dodecyl chain, 169 g/mol, and a density of 0.75 g/mL according to literature data for hydrocarbons gives a volume for the hydrophobic tail of a single molecule, V_{tail}, of 0.375 nm^3. This results in an aggregation number of 45 molecules for the smallest SDP2S micelles, considered as noninteracting hard spheres.

To determine the micellar diffusion coefficient D^{mic}, the measured diffusion coefficient was corrected by introducing the CMC and D^{mon} values into eq 1. The value of $D^{mon} = 4.27 \times 10^{-10}$ m^2/s was determined for six concentrations in the range from 0.1 to 0.05 mM. As expected, the diffusion coefficient does not depend on the surfactant concentration below CMC since the values for these samples appear equal within the experimental error. Figure 3 shows the concentration dependence of the $R_{h,app}$ calculated from eq 2, using either directly the measured diffusion coefficient, D^{meas} (dots), or the micellar diffusion coefficient, D^{mic} (squares), assuming that the concentration of the free surfactant above CMC is constant and equal to CMC. The curves reveal a nonlinear increase of $R_{h,app}$ upon increasing the surfactant concentration from 6 to 133 mM, which appears more pronounced for the data calculated directly from D^{meas}. For ionic surfactants, the assumption that the monomer concentration is constant above CMC is reasonable only for concentrations sufficiently close to CMC. However, at higher concentrations, the concentration of the free surfactant decreases as a consequence of increased counterion concentration.[25,26] Figure 3 shows that after substitution of D^{meas} (dots) for D^{mic} (squares), accounting for the monomer contribution, the apparent hydrodynamic radius tends to level off toward the two higher concentrations of 77.5 and 133 mM. At higher concentrations, micellar growth, the presence of attractive intermicellar interactions, and/or possible formation of nonspherical micelles, due to increasing micelle aggregation number, can explain the observed nonlinearity.

The properties of SDP2S solutions in the presence of multivalent ions, Ca^{2+} and Al^{3+}, have been previously investigated by dynamic and static light scattering.[9−11] A similar nonlinear dependence of the apparent micellar hydrodynamic radius on surfactant concentration for the concentration range from 1.5 to 8 mM was observed for SDP2S micelles in the presence of electrolytes at various ionic strengths and was interpreted as an indication of change of the aggregation number of cylindrical micelles. It was shown that the multivalent ions induce a sphere-to-rod shape transition at a lower ionic strength when compared to the monovalent electrolytes. The CMC values were found to be lower (0.13 mM for an ionic strength of 0.024 M) than the value in our study in the absence of additives.

3.3. Triton X-100. In the present study, the characteristics of TX100 micelles were investigated in a broad concentration range from 1.5 to 527 mM, which determines the boundaries of isotropic phase solution for this surfactant. Figure 4 shows the concentration dependence of the micellar diffusion coefficients (D^{mic}), calculated from eq 1a, using CMC = 0.25 mM and $D^{mon} = 2.85 \times 10^{-10}$ m^2/s as determined in the present study. The value of D^{mon} was measured for three samples with concentrations 0.1, 0.05, and 0.01 mM, far below the CMC of TX100. The micellar diffusion coefficients D^{mic} show a relatively weak dependence on surfactant concentration and display a reasonably linear decrease from 5.17×10^{-11} m^2/s to 2.92×10^{-11} m^2/s upon increasing the surfactant concentration up to ca. 77.5 mM (inset in Figure 4). Above this value, the concentration dependence is no longer linear. The observed nonlinear decrease of D^{mic} at high concentrations can be explained with concentration induced changes in micellar size, shape, and hydration. At concentrations above 77.5 mM, the presence of attractive intermicellar interactions leads to enhanced micellar growth, and possible agglomeration of micelles to larger globular particles, which could also explain the observed nonlinearity.[13,14]

Data set (1) in Figure 5 illustrates the evolution of the apparent micellar hydrodynamic radii ($R_{h,app}$), calculated using eq 2, as a function of the surfactant concentration. The calculations were restricted to the concentration range in which

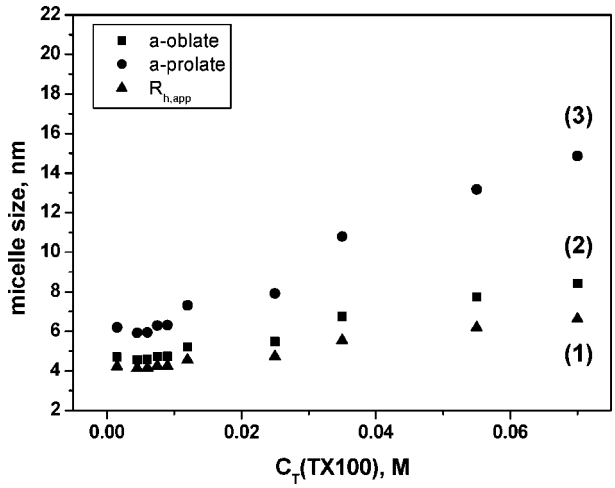

Figure 5. TX100 micelle size as a function of surfactant concentration, calculated using various shape factors: (1) apparent hydrodynamic radius, $R_{h,app}$, assuming spherical shape; major semiaxis length a assuming oblate (2) and prolate (3) ellipsoid shape factors.

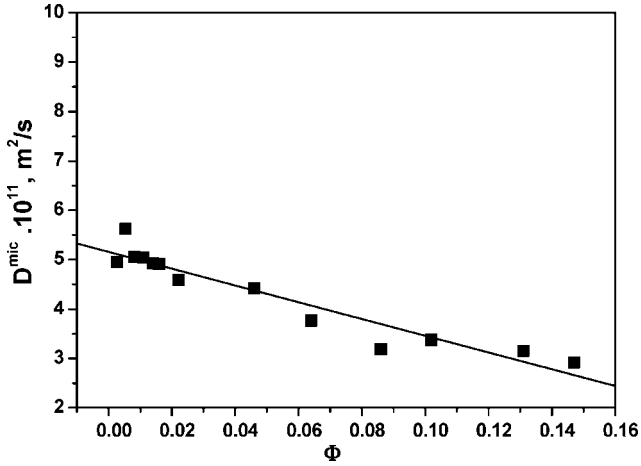

Figure 6. Micellar diffusion coefficient, D^{mic}, of TX100 as a function of micelle molar fraction Φ. ($R^2 = 0.9130$, Int $= 5.20 \pm 0.11 \times 10^{-11}$; Slope $= -1.69 \pm 0.16 \times 10^{-10}$, $N = 12$, SD $= 2.7758 \times 10^{-12}$, $N = 13$).

linear dependence of D^{mic} was observed (up to 77.5 mM). The apparent hydrodynamic radii increase from 4.2 to 7.2 nm. In principle, for moderate surfactant concentrations, the dependence of $R_{h,app}$ on the concentration is linear and can be attributed to an increase of micellar size.

At high concentrations, the volume fraction of the micelles in the solution increases, and micelle diffusion gets increasingly obstructed. Equation 6 was used in order to assess the possible existence of intermicellar interactions. Figure 6 shows the least-squares linear fit of D^{mic} to the molar fraction Φ, providing $D_0^{mic} = 5.17 \times 10^{-11}$ m^2/s as the y-intercept and $k = 3.5$ as the slope. Using eq 2 and the latter value of D_0^{mic}, we found a hydrodynamic radius at infinite dilution, $R_h = 4.01$ nm. These results are in an excellent agreement with literature values ranging from 3.2[13,14,17] to 4.5 nm,[15] as found by various methods. The value of k thus determined is slightly higher than generally accepted for hard sphere models. We interpret this result as some indication toward spheroid, slightly oblate, micelles. Alternative explanations for hard sphere deviation are the polydispersity of the oxyethylene chains resulting in an irregular distribution of the oxyethylene fragments in the micelle periphery, while the hydrocarbon core still remains spherical, as well as nonuniform hydration along the terminal oxyethylene chain.[12]

According to Phillies et al., who found an R_h value of 4.5 nm, this value is consistent with aggregation number of 97 monomers and hydration of approximately 2.6 g of water per gram of surfactant (4 water molecules per oxyethylene unit). However, the aggregation and hydration numbers found for TX100 in various papers are different and depend on the method used. Thus, from their intrinsic viscosity measurements, Robson and Dennis calculate a value of 1.2 g of water per gram of surfactant for a micelle radius of 4.3 nm, assuming an aggregation number of 143 monomers. TX100 formulations are known to be polydisperse and can display different molecular weight distributions when obtained from different sources, which can explain such discrepancies between literature data.

The issue of the shape of TX100 micelles is still open, an oblate or prolate ellipsoid being the two other possibilities under controversy.[12,16] Our data were also fitted with eqs 4 and 5 to oblate and prolate ellipsoids with the aim to calculate the axial ratio ρ. To simplify the calculations, we assumed that the minor semiaxis b is equal to the length of the surfactant molecule, which is a commonly accepted approximation. The total length of a TX100 molecule however depends on the conformation of the polyoxyethylene chain, which is not known, as the polyoxyethylene fragment has a relatively high degree of motional freedom, even in an aggregated state. To assess the length of the corresponding monomeric molecule, its geometry was optimized for the two limiting cases assuming meander and fully extended (zigzag) conformation of the polyoxyethylene chain (ab initio calculations at the B3LYP/6-31G level of theory, GAUSSIAN 98).[27] The dimension of the hydrophobic region (*p-tert*-octylphenyl group) was estimated to 0.94 nm, while the length of the oxyethylene chain constituted of 9.5 oxyethylene units was determined to be 3.3 nm in the zigzag and 2.3 nm in the meander conformation. Robson and Dennis[12] used values of 3.6 and 1.7 nm, respectively, the latter value being very close to the random coil dimension estimated to 1.6 nm. They assume further the dimension of the hydrophobic region (*p-tert*-octylphenyl group) to be 1 nm, which results in 2.7 nm total length for the surfactant molecule in the meander conformation, the value used in their work. According to other literature data,[28] the oxyethylene units adopt a zigzag conformation in a more hydrophobic environment, while in a hydrophilic medium the meander conformation is preferred. To assess the influence of the local environment on the conformation of the polyoxyethylene chain, we also performed ab initio calculations assuming zigzag conformation for the first four oxyethylene groups attached to the phenyl ring, which, being closer to the micellar core, are in a more hydrophobic environment. For the remaining five oxyethylene units in the periphery of the micelle, the meander geometry was adopted. With such a geometry, the polyoxyethylene chain length was calculated to be 2.5 nm, comparable to the fragment dimension if only a meander conformation is assumed. Thus, the total length, i.e., the minor semiaxis b, of the TX100 molecule used in our study is 3.3 nm. The results are gathered in data sets (2) and (3) of Figure 5, reflecting the concentration dependence of the semiaxis length a for the oblate and prolate ellipsoids, respectively, calculated using eqs 4 and 5, with $b = 3.3$ nm.

The results for assumed oblate ellipsoids, in the concentration region from 1.5 to 25 mM, show a very slight increase of the axial ratio ρ from 1.4 to 1.7 nm and the major semiaxis a from 4.6 to 5.5 nm, in agreement with Robson and Dennis[12] who found $\rho = 1.5$ and $a = 5.2$ nm. For concentrations above 25 mM, a monotonous increase of both ρ and a was observed.

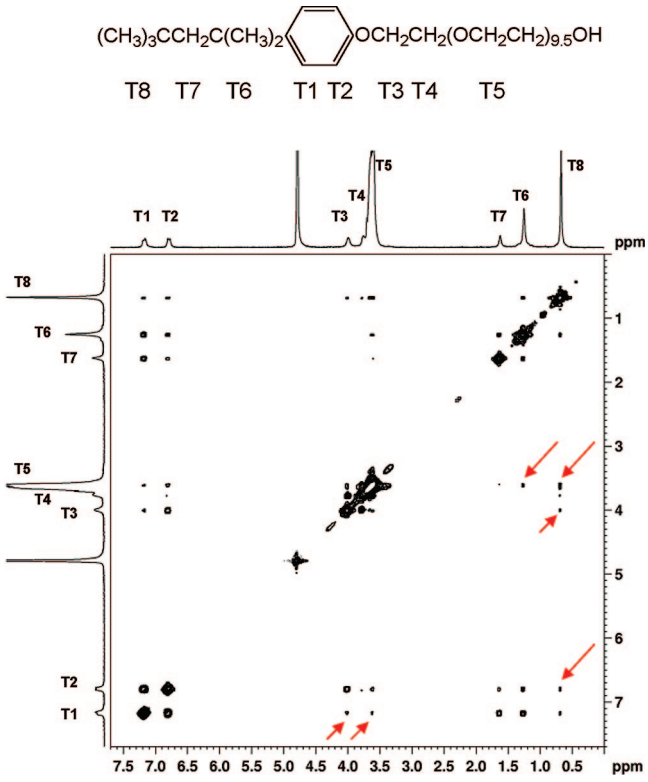

Figure 7. 2D NOESY spectrum of TX100 at $C_T = 9$ mM and mixing time $\tau_{mix} = 200$ ms. Some key cross-peaks are indicated with arrows.

Our results from DOSY NMR for prolate ellipsoids differ substantially from those of Robson and Dennis at low concentrations up to 25 mM. At higher surfactant concentration, however, the calculated values of the major semiaxis a ($\rho = 3.3 - 5.1$, $a = 10.8 - 16.9$ nm) do approach the value proposed by Robson and Dennis ($\rho = 5.2$, $a = 14.0$).[12]

3.4. NOESY Spectra: Triton X-100 Structure Investigation. With the aim to find further evidence enabling us to discriminate between the spherical and oblate models, 2D NOESY spectra[29−32] were recorded at surfactant concentrations of 9, 12, and 77.5 mM. The basis to our structural investigation starts from the still open proposal of Robson and Dennis[17] that if TX100 micelles are spherical they should have a multilayer structure, with partially overlapping internal and external layers of TX100 molecules, but if they are oblate shaped, the aggregates can only feature a monolayer structure. Regev and Zana[16] provide cryo-TEM evidence that TX100 micelles are spheroidal and comment that this should imply their dioxyethylene moieties to partially mix with nonpolar groups. It is precisely on this issue about TX100 that our 2D NOESY data below provide firm evidence.

The 2D NOESY spectrum of TX100 at $C_T = 9$ mM and a mixing time of 200 ms is shown in Figure 7, together with the molecular chain labeling used. The key cross-peaks revealing the proximity of some essential proton pairs are pointed out with arrows. Similar results were obtained at 12 and 77.4 mM.

Thus, 2D NOE cross-peaks correlate resonances from the terminal CH_3 groups (T8) and the aromatic protons in the *meta* position (T2) with respect to the *p-tert*-octylphenyl fragment. In addition to this T8−T2 cross-peak, two other key cross-peaks are between the aromatic T1 protons and the dioxyethylene protons T3, T4, and T5 (Figure 7). That these cross-peaks might originate from intramolecular interactions can be unambiguously ruled out since the key cross-peaks T8−T2, T1−T3, and T1−T4 are absent in the 2D NOESY spectrum of the nonmicellar TX100 surfactant. Thus, the intermolecular origin of these key NOE contacts is undisputable. Representative cross-sections of the 2D NOESY spectrum at the chemical shifts of the two aromatic protons T1 and T2 at a mixing time of 250 ms are given in the Supporting Information (Figure S1).

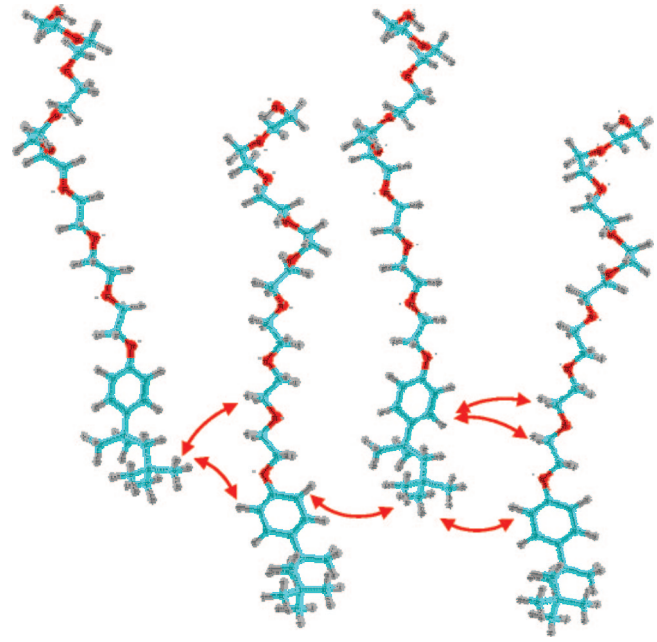

Figure 8. Spatial arrangement of the TX100 surfactant molecules in the micellar state matching the through-space interactions revealed by the 2D NOESY cross-peaks. The key intermolecular NOE contacts are indicated with arrows.

We further support the interpretation of the T8−T2 cross-peak as raising from intermolecular interactions, with relaxation time measurements on the hydrophobic chain proton resonances indicating a relatively high degree of conformational mobility, even in the micelle ($T_1 = 230$ ms for T8, 350 ms for T2, and 430 ms for T1; $T_2 = 120$ ms for T8, 105 ms for T2, and 100 ms for T1).

Further, cross-peaks arising from intermolecular interactions, only interpretable with a double layer structure, correlate resonances of the terminal methyl groups T8 from the second (outer) layer to those of the first three methylene groups (T3, T4, T5) from the oxydiethylene chain of the first (inner) layer.

To eliminate any spin-diffusion effects as a possible mechanism contributing to the observed NOE correlations, the cross-peak intensity was measured as a function of mixing time. The key cross-peak intensities increase linearly upon increasing mixing time from 5 to 200 ms, show a maximum around 300 ms, and start to decrease upon further increase of the mixing time. As an example, the evolution of the T8−T2 cross-peak intensity as a function of mixing time is represented in Figure S2 in the Supporting Information. The observed linear dependence of the cross-peak intensity at short mixing times and the lack of induction period unambiguously exclude spin diffusion.

All these 2D cross-peak patterns evidence that the surfactant molecules are arranged in at least two layers with the *p-tert*-octylphenyl fragment of the outer layer facing the first three oxyethylene groups of the inner layer. The mutual spatial arrangement of four neighboring surfactant molecules in the micelle, matching all these 2D NOESY cross-peaks, is schematically presented in Figure 8. The key intermolecular NOE contacts are indicated with arrows.

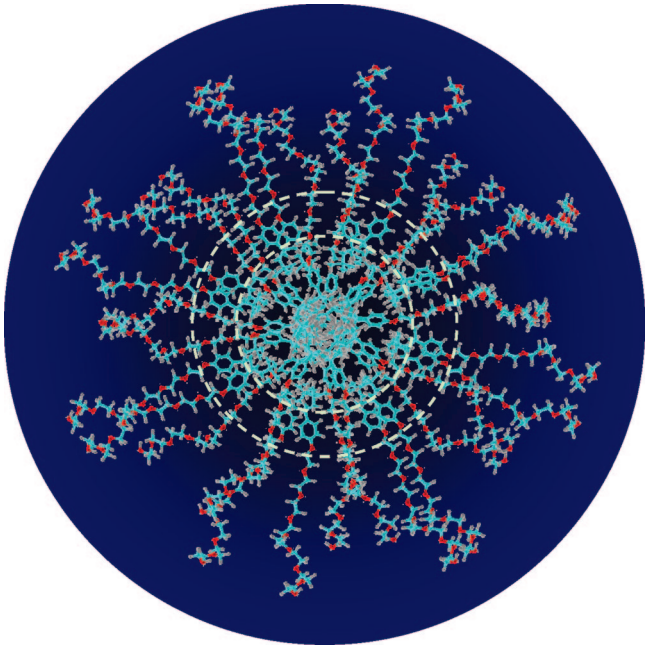

Figure 9. Simplified schematic representation of TX100 micelle structure based on cross-relaxation effects observed in the 2D NOESY spectrum.

A simplified schematic representation of the TX100 micelle structure in the low concentration limit up to 77.5 mM is proposed in Figure 9. The micelle region to which the above NOESY data are relevant is confined within the two dashed circles. This region can be considered as the transition area between the hydrophilic and hydrophobic domains of the aggregates. Figure 9 is only a schematic representation of the micelle for which no data are available for the those areas outside the dotted circle. This means, in particular, that the data at hand cannot provide evidence as to the questions whether this micellar aggregate is double- or multilayered, on the one hand, and how the molecular arrangement appears in the center of the micelle aggregate.

Conclusions

Our ^{1}H NMR results reveal that the individual Triton X-100 and SDP2S micelles have approximately spherical shapes. The hydrodynamic radius, R_h, of Triton X-100 micelles increases linearly from 4 to 7 nm, upon increasing surfactant concentration in the low concentration range (1.5−100 mM). For the same concentration range, the individual SDP2S micelles are smaller, with the R_h value increasing nonlinearly from 3 to 5 nm. The CMC of 0.8 mM was determined for SDP2S in the absence of additives. The combined application of DOSY and NOESY NMR enabled us to characterize the micelle size and shape, getting insight into the mutual spatial arrangement of surfactant molecules in the TX100 micelles. The results from NOESY spectra show that TX100 micelles are spherical and have at least a double layer structure, with no well-marked hydrophilic−hydrophobic boundary.

Acknowledgment. The financial support by the Fund for Scientific Research-Flanders (FWO, Belgium) for the scientific exchange stay of PSD at the High Resolution NMR Centre of the Vrije Universiteit Brussel (VUB), Belgium, and by the National Science Fund (Grant X-1408), Ministry of Education and Science, Bulgaria, is gratefully acknowledged. PSD and LVL are indebted to the fund of Scientific Research Flanders (Belgium) (FWO) and the Bulgarian Academy of Sciences (BAS), for bilateral scientific exchange fellowships at VUB and BAS (Grant VS.013.07N). R.W. is indebted to the Fund for Scientific Research-Flanders (FWO, Belgium) for financial support (Grant G.0064.07) and to the Research Council (Onderzoeksraad) of the Vrije Universiteit Brussel for financial support (Concerted Research Action, Grant GOA31 and other grants), of the postdoctoral stay of PSD and the PhD of L.V.L.

Supporting Information Available: Figures S1 and S2. This material is available free of charge via the Internet at http://pubs.acs.org.

References and Notes

(1) Israelachvili, J. N. *Intermolecular and Surface forces*; Academic Press: London, 1991.
(2) Evancs, D. F.; Winnerström, H. *The Colloidal Domain: Where Physics, Chemistry, Biology, and Technology Meet*; VCH Publishers, Inc.: New York, 1994.
(3) Lindman, B.; Olsson, U.; Söderman, O. *Dynamics of Solutions and Fluid Mixtures by NMR*; Delpuech, J., Ed.; Wiley: Chichester, 1995; Chapter 8.
(4) Söderman, O.; Stilbs, P. *Prog. Nucl. Magn. Reson. Spectrosc.* **1994**, *26*, 445.
(5) Söderman, O.; Stilbs, P.; Price, W. *Concepts Magn. Reson. A* **2004**, *23*, 121.
(6) Stilbs, P. *Prog. Nucl. Magn. Reson. Spectrosc.* **1987**, *19*, 1.
(7) Johnson, C. S., Jr. *Prog. Nucl. Magn. Reson. Spectrosc.* **1999**, *34*, 203.
(8) Antalek, B. *Concepts Magn. Reson.* **2002**, *14*, 225.
(9) Alargova, R.; Petkov, J.; Petsev, D.; Ivanov, I. B.; Broze, G.; Mehreteab, A. *Langmuir* **1995**, *11*, 1530.
(10) Alargova, R.; Ivanova, V. P.; Kralchevsky, P. A.; Broze, G.; Mechreteab, A. *Colloids Surf. A* **1998**, *142*, 201.
(11) Alargova, R.; Danov, K. D.; Kralchevsky, P. A.; Broze, G.; Mechreteab, A. *Langmuir* **1998**, *14*, 4036.
(12) Robson, R.; Dennis, E. *J. Phys. Chem.* **1977**, *81*, 1075.
(13) Brown, W.; Rymden, R.; van Stam, J.; Almgren, M.; Svensk, G. *J. Phys. Chem.* **1989**, *93*, 2512.
(14) Sadaghiani, A. S.; Khan, A. *Langmuir* **1991**, *7*, 898.
(15) Phillies, G. D. J.; Lambert, J. E. *Langmuir* **1996**, *12*, 3431, and references therein.
(16) Regev, O.; Zana, R. *J. Colloid Interface Sci.* **1999**, *210*, 8.
(17) Molina-Bolivar, J. A.; Aguiar, J.; Ruiz, C. C. *J. Phys. Chem. B* **2002**, *106*, 870.
(18) Wu, D.; Chen, A.; Johnson, C. S., Jr. *J. Magn. Reson. A* **1995**, *115*, 260.
(19) Jershow, A.; Müller, N. *J. Magn. Reson.* **1997**, *125*, 372.
(20) Delsuc, M. A.; Malliavin, T. E. *Anal. Chem.* **1998**, *70*, 2146.
(21) Hiemenz, P. C. *Principles of Colloid and Surface Chemistry*; Marcel Dekker: New York, 1986.
(22) Lekkerkerker, H. N. W.; Dhont, J. K. J. *J. Chem. Phys.* **1984**, *80*, 5790.
(23) Medina-Noyola, M. *Phys. Rev. Lett.* **1988**, *60*, 2705.
(24) Nydén, M.; Söderman, O. *Langmuir* **1995**, *11*, 1537.
(25) Stilbs, P.; Lindman, B. *J. Phys. Chem.* **1981**, *85*, 2587.
(26) Lindman, B.; Puyal, M. C.; Kamenka, N.; Rymdén, R.; Stilbs, P. *Phys. Chem.* **1984**, *88*, 5048.
(27) Frisch, M. J.; Trucks, G. W.; Schlegel, H. B.; Scuseria, G. E.; Robb, M. A.; Cheeseman, J. R.; Zakrzewski, V. G., Montgomery, J. A., Jr.; Stratmann, R. E., Burant, J. C., Dapprich, S.; Millam; J. M.; Daniels, A. D.; Kudin, K. N.; Strain, M. C.; Farkas, O.; Tomasi, J.; Barone, J.; Cossi, M.; Cammi, R.; Mennucci, B.; Pomelli, C.; Adamo, C.; Clifford, S.; Ochterski, J.; Petersson, G. A.; Ayala, P Y.; Cui, Q.; Morokuma, K.; Malick, D. K., Rabuck, A. D.; Raghavachari, K.; Foresman, J. B.; Cioslowski, J., Ortiz, J. V.; Baboul, A. G.; Stefanov, B. B.; Liu, G.; Liashenko, A.; Piskorz, P.; Komaromi, I.; Gomperts, R.; Martin, R. L., Fox, D. J., Keith, T., Al-Laham, M. A., Peng, C. Y., Nanayakkara, A., Gonzalez, C., Challacombe, M., Gill, P. M. W., Johnson, B., Chen, W., Wong, M. W., Andres, J. L., Gonzalez, C., Head-Gordon, M., Replogle, E. S., Pople, J. A., *Gaussian 98, Revision A.7*; Gaussian, Inc.: Pittsburgh, PA, 1998.
(28) Ribeiro, A. A.; Dennis, E. A. *Nonionic Surfactants: Physical Chemistry*; Schick, M. J., Ed.; Marcell Dekker: New York, 1987; Chapter 17.
(29) Neuhaus, D.; Williamson, M. *The Nuclear Overhauser Effect in Structural and Conformational Analysis*; Wiley-VCH: New York, 2000.
(30) Rozycka-Roszak, B.; Cierpicki, T. *J. Colloid Sci.* **1999**, *21*, 8–529.
(31) Yuan, H.; Cheng, G.; Zhao, S.; Miao, X.; Yu, J.; Shen, L.; Du, Y. *Langmuir* **2000**, *16*, 3030.
(32) Emin, S. M.; Denkova, P. S.; Papazova, K. I.; Dushkin, C. D.; Adachi, E. *J. Colloid Interface Sci.* **2007**, *305*, 133.

JP802830G